Journal of Sound and Vibration (1997) **203**(2), 283–305

IDENTIFICATION OF DAMPING IN MDOF SYSTEMS USING TIME-SCALE DECOMPOSITION

W. J. Staszewski

Dynamics Research Group, Department of Mechanical Engineering, University of Sheffield, Mappin Street, Sheffield S1 3JD, England

(*Received* 18 *June* 1996, *and in final form* 25 *November* 1996)

A method of damping identification in multi-degree-of-freedom systems is presented. The method is based on the time-scale decomposition of the system impulse response. The continuous wavelet transform is used to decompose the impulse response into the time-scale domain. Three techinques based on the wavelet transform are used to estimate damping. These are the wavelet transform cross-section procedure, the impulse response recovery procedure based on wavelet domain filtering and the wavelet ridge detection procedure. The methods are applied to simulated multi-degree-of-freedom systems.

1. INTRODUCTION

Damping is a mechanism that dissipates vibration energy in dynamic systems. Structures and machinery can be damped by mechanisms which have different internal and external natures. These include for example, atomic/molecular microstructure effects, friction between parts, impacts and air/fluid interactions. A combination of different phenomena results in various types of damping. In general, structural damping can be classified either as hysteretic or viscous [1]. Hysteretic damping arises from microstructural phenomena and is characterised by material properties. Viscous damping is proportional to velocity and affects the system response at or near resonances. In real structures many different types of damping act simultaneously; this in practice leads to the concept of equivalent viscous damping which models the overall damped behaviour of the system as being viscous. Different models are used to represent damping in structures. These models do not necessary imply the actual physical description of damping. The most basic models are modal damping [2] and Rayleigh damping [3].

A number of damping measures and criteria are used in practice to characterize structural damping [3, 4]. The damping ratio, or fraction of critical damping, is used in this paper to describe viscous damping.

It appears in practice that damping parameters in multi-degree-of-freedom (MDOF) systems are the most critical to estimate. It is well known that they are the most sensitive to noise, measurement errors, inadequate excitation, etc. There exist different techniques for measuring damping values and properties [4, 5]. Different methods of damping identification have also been developed in dynamics; a review can be found in references [4, 6]. These methods can be classified into time and frequency domain. The logarithmic decrement is the simplest time-domain method used for single-degree-of-freedom (SDOF) systems. More elaborate time-domain techniques are used for MDOF systems. The most popular techniques include the Smith least squares (SLS) algorithm [7] and the least squares complex exponential (LSCE) method [7] which basically fit the impulse response function (IRF) of a MDOF system. A modification of the SLS method based on an initial

0022–460X/97/220283 + 23 $25.00/0/sv960864

estimate obtained from the logarithmic decrement can be found in reference [6]. Other time domain techniques used for SDOF and MDOF systems include limit envelopes [8] and Hilbert transform [9–13].

Frequency domain methods are based on the frequency response function (FRF). The 3-dB method [3] uses the amplitude of the FRF. This method can be improved when the phase information from the Nyquist plot is used additionally [3]. The methods can be extended to MDOF systems for lightly coupled modes with minimal crossovers. They also give significant errors in the case of lightly damped systems. More accurate results can be obtained when curve-fitting techniques are applied to the FRF. This can be done by using, for example, a linear least squares technique for the SDOF system and a non-linear least squares technique for the MDOF system. A comparison between various time and frequency domain methods is given in reference [6]. A combined time-frequency approach can be applied to estimate the damping of the system by using, for example, the Wigner–Ville distribution [10, 13]. The main use of a time-frequency approach to the study of vibration signals is made on time variations of the spectral characteristics.

A different approach evolves if vibration signals are considered as a superposition of a number of components which are more or less localized. This can be done by using signal decomposition based on *a priori* chosen functions. Thus instead of a time-frequency representation one deals with a time-scale representation. The first work in this area goes back to Gabor [14] and Hoelström [15] who used shifted versions of Gaussian discrete and continuous functions in the time and frequency domains. If the time/frequency shift is replaced by a dialtion or compression of scale, the time-scale decomposition leads directly to the wavelet transform. The wavelet transform originated in the early 1980s in the works of Morlet [16] who used it in seismology and then Grossman and Morlet [17] who developed the geometrical formalism of the continuous wavelet transform. However, there is a relationship between these developments and the previous work of Calderon [18] in the area of mathematics, and Esteban and Galand [19] in signal processing. The method has been evolving rapidly for the last ten years. The historical background and major theoretical developments are reported, for example, in references [20, 21]. The wavelet transform has found many applications in different areas. Structural identification analyses are included in the references [22–27].

This paper presents three different damping estimation procedures for MDOF systems, based on the wavelet transform. For the sake of completeness the continuous wavelet transform is briefly introduced in section 2. Section 3 gives the main concept of damping estimation in MDOF systems by using the wavelet transform. Two models of damping together with the mode decoupling procedure are presented. A damping estimation procedure based on the wavelet transform cross-sections is described in section 4. Section 5 gives the impulse response function recovery based on wavelets. The concept of wavelet ridges and skeletons is presented in section 6. Finally, examples of damping identification in linear and non-linear MDOF systems is given in section 7.

2. THEORETICAL BACKGROUND OF THE WAVELET TRANSFORM

The theoretical formalism of the time-scale analysis transform is a result of similarities between methods developed in various fields from mathematics to signal precessing. For the sake of completeness, this section gives a basic presentation of the wavelet transform theory together with a summary of the most important properties used in the paper.

The Fourier transform can be considered as a decomposition of a function into a linear combination of vectors given by Fourier coefficients. This decomposition does not give any local information about the function due to the infinite nature of the trigonometric

functions used in the analysis. One of the most recent, rapidly evolving methods which provides for locality is the wavelet transform.

Suppose that all functions $x(t)$ satisfy the condition

$$\int_{-\infty}^{+\infty} |x(t)|^2 \, \mathrm{d}t < \infty, \tag{1}$$

which implies that $x(t)$ decays to zero at $\pm\infty$. The wavelet transform can be defined as

$$(W_g x)(a, b) = \frac{1}{\sqrt{a}} \int_{-\infty}^{+\infty} x(t) g^*\left(\frac{t-b}{a}\right) \mathrm{d}t, \tag{2}$$

where b is a translation indicating the locality, a is a dilation or scale parameter, $g(t)$ is an analyzing (basic) wavelet and $g^*(\cdot)$ is the complex conjugate of $g(\cdot)$. Each value of the wavelet transform $(W_g x)(a, b)$ is normalized by the factor $1/\sqrt{a}$. This normalization ensures that the integral energy given by each wavelet $g_{a,b}(t)$ is independent of the dilation a.

It can be seen now that the wavelet transform is an example of a linear transformation that decomposes an arbitrary function $x(t)$ into the elementary functions $g_{a,b}(t)$ which are obtained from the analyzing wavelet $g(t)$ by dilation and translation. The time decomposition is given by trnaslation b. The frequency segmentation, or in other words the scale decomposition, is obtained by dilating the chosen analyzing wavelet. Here dilation represents the harmonic or periodic nature in terms of harmonic/periodic decomposition. These two operations are sufficient to produce a basis which can represent any function in the entire analysis space. For practical purposes the decay given by equation (1) is very fast and thus introduces locality into the analysis. This is not the case for the Fourier transform, where one infinite trigonometric function gives a global representation.

The function $g(t)$ qualifies for an analyzing wavelet, when it satisfies the admissibility conditon [21]

$$C_g = \int_{-\infty}^{+\infty} \frac{|G(f)|^2}{|f|} \, \mathrm{d}f < \infty, \tag{3}$$

where $G(f)$ is the Fourier transform of $g(t)$. This is necessary for obtaining the inverse of the wavelet transform given by [21]

$$x(t) = \frac{1}{C_g} \int_{-\infty}^{+\infty} \int_{-\infty}^{+\infty} (W_g x)(a, b) \frac{1}{\sqrt{a}} g^*\left(\frac{t-b}{a}\right) \frac{\mathrm{d}a \, \mathrm{d}b}{a^2}. \tag{4}$$

The possibility of time-frequency localization arises from the $g(t)$ being a window function, which means that additionally [21]

$$\int_{-\infty}^{+\infty} |g(t)| \, \mathrm{d}t < \infty. \tag{5}$$

In practice, some regularity and smoothness of the wavelet function is also required.

There are a number of different complex and real valued functions used as analyzing wavelets. In many cases a so called progresive wavelet function is used, being a complex valued function that satisfies the admissibility conditon and does not have any negative

frequencies. The progressivity condition ensures that the wavelet transform does not produce any interference in the time domain between the past and the future. One of the most widely used functions in wavelet analysis is the Morlet wavelet defined by [28]

$$g(t) = e^{j2\pi f_0|t|}\, e^{-|t|^2/2} \tag{6}$$

The Fourier spectrum of the Morlet wavelet is a shifted Gaussian function [28]

$$G(f) = \sqrt{2}\pi\, e^{-2\pi^2(f-f_0)^2} \tag{7}$$

It can be seen that the admissibility condition given by expression (3) is not satisfied since $G(0) \geqslant 0$ which gives $C_g = +\infty$. In practice the value of $f_0 > 5$ is used [28] which meets approximately the requirements given by condition (3). Another way to impose admissibility is to set $G(0) = 0$ or even $G(f) = 0$ for $f \leqslant 0$. The latter causes the Morlet wavelet to be progressive.

Figure 1 shows an example of the Morlet wavelet function in the time and frequency domain for different values of dilation parameters. In many cases the so called shifted Morlet wavelet can be used. Thus instead of f in equation (7), $f - f_h$ is applied, where f_h is the shift frequency of the Morlet wavelet. When the shifted Morlet wavelet is used, the frequency position of the wavelet function is changed but its frequency bandwidth remains unchanged which gives better time resolution of the wavelet function.

The wavelet transform has a number of useful properties which have been widely analyzed and can be found elsewhere; e.g. in reference [21]. In what follows, a summary of the most important properties which are used in this work, is given.

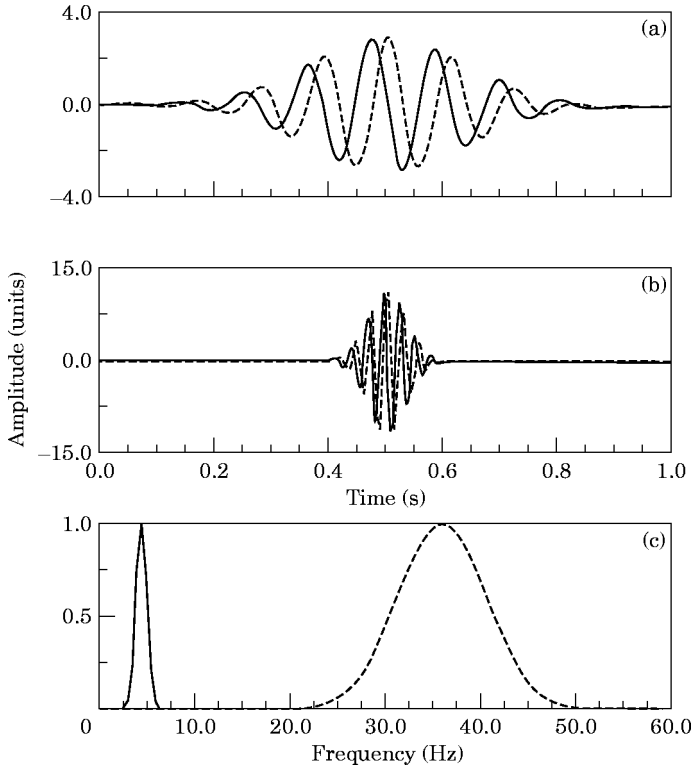

Figure 1. An example of the Morlet wavelet function in the (a,b) time and (c) frequency domains. —, real part; – – –, imaginary part.

The wavelet transform is a linear representation of a signal. Thus it follows that for a given N functions x_i and N complex values $\alpha_i (i = 1, 2, \ldots, N)$

$$\left(W_g \sum_{i=1}^{N} \alpha_i x_i \right)(a, b) = \sum_{i=1}^{N} \alpha_i (W_g x_i)(a, b). \tag{8}$$

This property is convenient for the analysis of multi-component signals.

It is clear from the definition that the Fourier transform extracts periodic infinite waves from the analyzed function. In contrast, the wavelet transform analyzes a function only locally at windows defined by a wavelet function. Equation (2) is in general non-local. The value of $(W_g x)(a, b)$ at a point (a_0, b_0) depends on $x(t)$ for all t. However conditions (1) and (5) provide that the function $g(t)$ decays to zero at $-\infty$ and $+\infty$. If one assumes a fast decay, i.e., the values of $g(t)$ are negligible outside the interval (t_{min}, t_{max}), the transform becomes local. This feature has been explained in detail in reference [21].

The frequency localization is clearly seen when the wavelet transform is expressed in terms of the Fourier transform,

$$(W_g x)(a, b) = \sqrt{a} \int_{-\infty}^{+\infty} X(f) G^*_{a,b}(af)\, \mathrm{e}^{\mathrm{j}2\pi fb}\, \mathrm{d}f, \tag{9}$$

where $G^*(\cdot)$ is the complex conjugate of $G(\cdot)$. This localization depends on the dilation parameter a. The local resolution of the wavelet transform in time and frequency is determined by the duration and bandwidth of analyzing functions given by [21]

$$\Delta t = a \Delta t_g, \qquad \Delta f = \Delta f_g / a, \tag{10}$$

where Δt_g and Δf_g are the duration and bandwidth of the basic wavelet function, respectively. Thus, in the frequency domain, the wavelet transform has good resolution at high dilations and hence low frequencies (see below) and in the time domain good resolution at high frequencies, the latter being suitable for non-stationary and transient signal detection.

The wavelet transform as a signal decomposition cannot be directly compared to any time-frequency representation. However there is a relationship betwen dilation and frequency. For the Morlet analyzing wavelet function, the relationship between the dilation parameter a_f and the signal frequency f_x at which the analyzing wavelet function is focused, can be given as [29]

$$a_f = f_0 \, (f_s / f_w) \, (1 / f_x), \tag{11}$$

where f_s and f_w are the sampling frequencies of the signal and the analyzing wavelet, respectively.

The frequency bandwidth of the wavelet function for the given dilation a can be obtained using a frequency representation of the Morlet wavelet and expressed as

$$\Delta f_x = (1 / \pi a)(f_s / f_w). \tag{12}$$

This allows one to obtain a single element of the wavelet decomposition of the function for a given value of frequency (dilation) and frequency bandwidth.

3. DAMPING ESTIMATION IN MDOF SYSTEMS USING WAVELETS

3.1. BACKGROUND

The linear MDOF system is governed by the general equation

$$[\mathbf{M}]\ddot{X} + [\mathbf{C}]\dot{X} + [\mathbf{K}]X = \mathbf{F}, \tag{13}$$

where [**M**], [**C**], [**K**], are mass, damping and stiffness matrices respectively, and **F** is the excitation vector. The response X of the system can be obtained by using well known modal analysis or a direct forced response method. Modal analysis involves the calculations of eigenvalues and eigenvectors for the undamped system. The eigenvectors can then be used to transfer equation (13) into modal space involving modal mass, damping and stiffness matrices. The direct forced response approach uses the direct solution of equation (13) without any eigenanalysis. Both approaches require damping to be defined in order to obtain the damped response of the system. In practical applications different classes of damping introduced in section 1 are difficult to use. Thus the concept of equivalent viscous damping has been introduced. This implies that the overall behaviour of the structure is modelled as viscous. The same amount of energy is assumed to be dissipated at resonances and thus the concept is valid only for SDOF systems. Indeed, mathematically equation (13) is in general a set of N coupled equations. However, the concept of equivalent damping can be generalized for MDOF systems by using different models of damping. The modal damping approach uses the damping ratio ζ for a SDOF system. This can be generalized for an MDOF system when the damping ratio is applied to all modes in the modal space. Alternatively the uncoupled solution of equation (13) is possible by using the Rayleigh damping model. This model assumes [**C**] to be linearly proportional to [**M**] and [**K**].

3.2. WAVELET BASED MODE DECOUPLING PROCEDURE

Modal analysis and direct forced response approaches together with damping models described in section 3.1. can lead to uncoupling of MDOF systems.

Instead of the MDOF system given by equation (13), N uncoupled equations similar to a SDOF system can be obtained,

$$m_i\ddot{x}_i(t) + c_i\dot{x}_i(t) + k_i x_i(t) = f_i(t), \tag{14}$$

for $i = 1, 2, \ldots, N$. In practice these uncoupled equations can also be obtained when the damping is assumed to be small. The impulse response of this MDOF system can be given in general form as

$$h(t) = \sum_{i=1}^{N} A_i \, \mathrm{e}^{-\zeta_i \omega_{n_i} t} \sin\left(\sqrt{1-\zeta_i^2}\,\omega_{n_i} t + \psi_i\right), \tag{15}$$

where ω_{n_i} is the natural frequency, N is the number of modes considered, A_i is the residue magnitude of the ith mode and ζ_i is the damping ratio. This response represents a linear combination of its single modal components. Each mode is given by an exponentially decaying harmonic function.

It has been shown in section 2 that the wavelet transform is a signal decomposition procedure working as a filter in the time-frequency domain. Thus it offers a possible means of uncoupling vibration modes. Since the analyzing wavelet function has compact support in the time and frequency domains, equation (2) can be re-written for multi-component signals, by using equation (10), as

$$\left(W_g \sum_{i=1}^{N} x_i\right)(a, b) = \frac{1}{\sqrt{a}} \sum_{i=1}^{N} \int_{t-a\Delta t_g}^{t+a\Delta t_g} x_i(t) g^*\left(\frac{t-b}{a}\right) \mathrm{d}t. \tag{16}$$

From equations (9) and (10) this can be expressed in the frequency domain as

$$\left(W_g \sum_{i=1}^{N} x_i\right)(a, b) = \sqrt{a} \sum_{i=1}^{N} \int_{f_i - \Delta f_g/a}^{f_i + \Delta f_g/a} X(f) G^*_{a,b}(af)\, \mathrm{e}^{\mathrm{j}2\pi f b}\, \mathrm{d}f \tag{17}$$

The wavelet analyzing function for each ith mode is peaked at modal frequency f_i. For the Morlet wavelet function the relationship between frequency and dilation, and the frequency bandwidth of the filter are given by equations (11) and (12), respectively.

The following sections give three methods of damping estimation based on the wavelet transform uncoupling procedure.

4. DAMPING IDENTIFICATION USING WAVELET TRANSFORM CROSS-SECTIONS

For the simple case of a SDOF system

$$m\ddot{x}(t) + c\dot{x}(t) + kx(t) = f(t), \tag{18}$$

the impulse response function is given as

$$h(t) = A_0\, \mathrm{e}^{-\zeta\omega_n t} \sin\left(\sqrt{1 - \zeta^2}\omega_n t + \xi\right) \tag{19}$$

where ω_n is the natural frequency, A_0 is the residue magnitude and ζ is the damping ratio. Here the oscillating term is given by a sine wave at the damped natural frequency and the damping is represented by the exponentially decaying envelope. It is well known that the dissipative mechanism of the system can be detected by the analysis of the decaying envelope $A(t)$ of the impulse response function. For the system given by equation (18) the constitutive function $A(t)$ is known in the explicit form

$$A(t) = A_0\, \mathrm{e}^{-\zeta\omega_n t}, \tag{20}$$

where $\zeta = 2c\sqrt{km}$, m and k are mass and stiffness of the system respectively. The envelope function $A(t)$ can be obtained by using the approach based on the Hilbert transform [30]. After a simple calculation, it is revealed that

$$\ln\left(A(t)\right) = -\zeta\omega_n t + \ln\left(A_0\right), \tag{21}$$

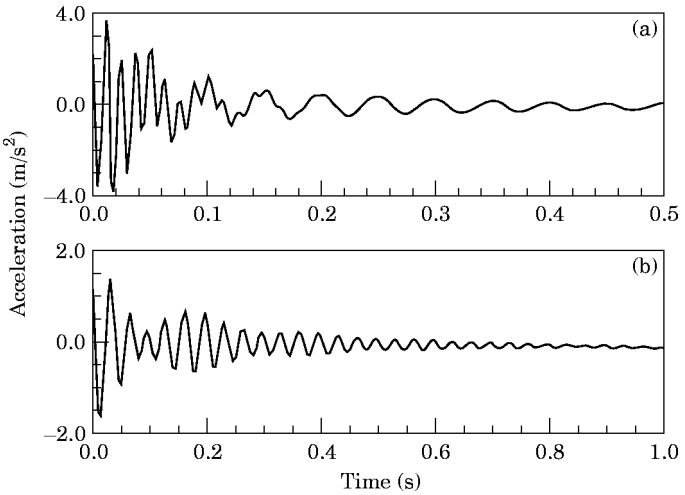

Figure 2. Impulse response functions. (a) Well separated modes from Example 1; (b) close modes from Example 2.

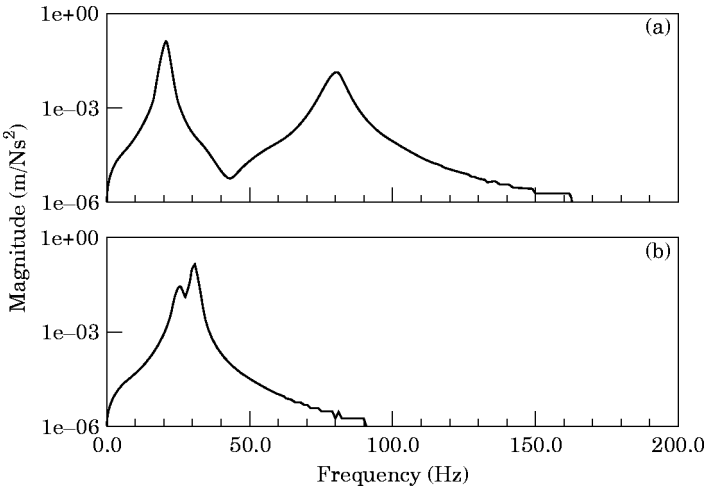

Figure 3. Frequency response functions: (a) Well separated modes from Example 1; (b) close modes from Example 2.

Thus the damping ratio ζ of the system can be estimated from the slope of the straight envelope line $A(t)$ plotted in a semi-logarithmic scale. This procedure is well known in the literature and applications can be found elsewhere [4, 10].

A similar procedure can be applied in the case of the wavelet transform. Consider again the SDOF system given by equation (18). When the damping term $(c/2m)^2$ is less than the stiffness k/m the solution of the system can be given in the form of an analytic signal

$$x(t) = A(t)\, \mathrm{e}^{\pm \mathrm{j}\omega_n \sqrt{1-\zeta^2} t} = A(t)\, \mathrm{e}^{\mathrm{j}\phi(t)} \tag{22}$$

Assume that the envelope $A(t)$ is slowly varying. For the Morlet wavelet function $g(t)$ given by equation (6), which is also an analytic complex valued function and has good localization properties in the frequency domain, the wavelet transform of the solution (22) can be approximated as [31]

$$(W_g x)(a, b) \approx A(b) G^*((a\dot{\phi}(b)))\, \mathrm{e}^{\mathrm{j}\phi(b)} + o(|\dot{A}|, |\ddot{\phi}|), \tag{23}$$

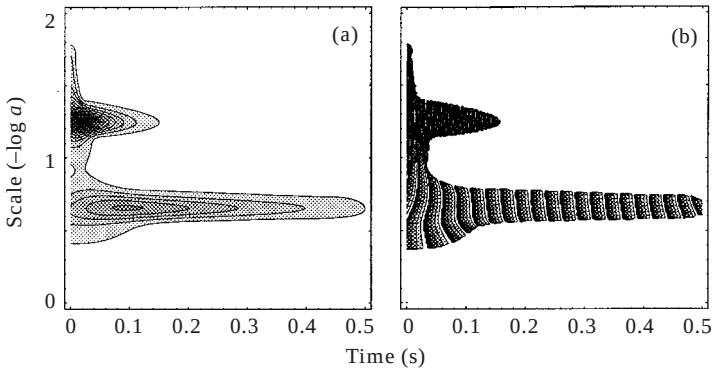

Figure 4. Wavelet transform for the impulse response function from Example 1 representing well separated modes. (a) Amplitude; (b) phase.

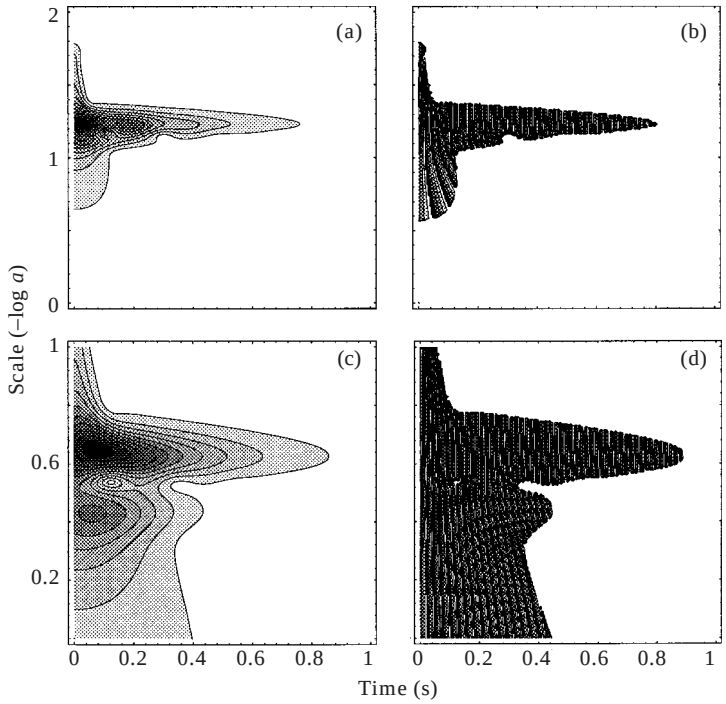

Figure 5. Wavelet transform for the impulse response function from Example 2 representing close modes. The Morlet (a,b) and shifted Morlet (c,d) wavelet functions were used in the analysis. Key: (a), (c) amplitude; (b), (d) phase.

where $G^*(\cdot)$ denotes the complex conjugate of $G(\cdot)$. The modulus of this function is given by

$$|(W_g x)(a, b) \approx A(b)|G^*(a\dot{\phi}(b))|. \tag{24}$$

For a given value of dilation a_0, from equations (20), (22) and (24), the following can be obtained:

$$|(W_g x)(a_0, b) \approx A_0 \, \mathrm{e}^{-\zeta\omega_n b}|G^*(\pm a_0 \mathrm{j}\omega_n\sqrt{1-\zeta^2})|. \tag{25}$$

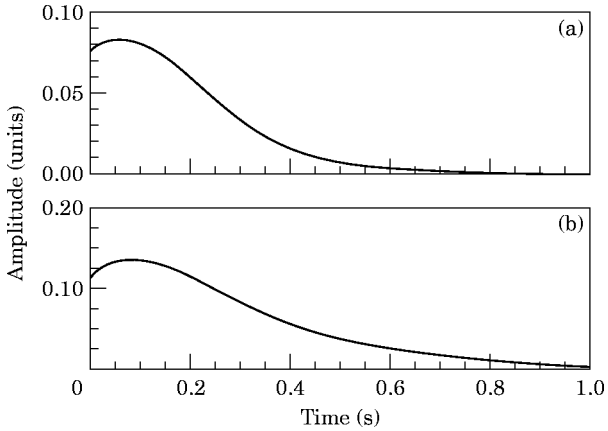

Figure 6. Cross-sections of the wavelet transform amplitude representing the impulse response function with close modes from Example 2. The values of dilation for the cross-sections were chosen to match the frequencies of the analysed modes. (a) first mode (25 Hz); (b) second mode (30 Hz).

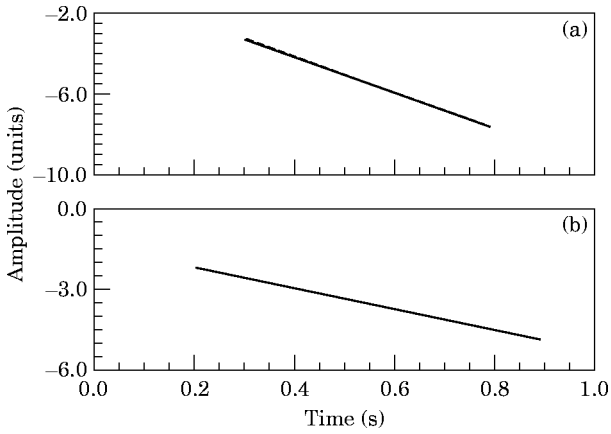

Figure 7. Semi-logarithmic plots of the cross-sections given in Figure 6: (a) First mode (25 Hz); (b) second mode (30 Hz).

When the logarithm is applied to equation (25), a simple calculation shows

$$\ln (W_g x)(a_0, b)| \approx -\zeta\omega_n b + \ln (A_0|G^*(\pm \mathrm{j}a_0\omega_n\sqrt{1-\zeta^2})|). \tag{26}$$

Thus the damping ratio ζ of the system can be estimated from the slope of the straight line of the wavelet modulus cross-section $|(W_g x)(a_0, b)|$, for the given value of dilation a_0, plotted in a semi-logarithmic scale. This result is similar to the envelope analysis given by equation (21). Equation (26) is restricted to complex valued analytic signals. However, in the case of real valued signals of the form

$$x(t) = A(t)\cos\phi(t), \tag{27}$$

when the progressive Morlet wavelet function $g(t)$ is used, the corresponding wavelet transform is given by [31]

$$(W_g x)(a, b) = \langle x(t), g_{a,b}(t)\rangle = \tfrac{1}{2}\langle x_a(t), g_{a,b}(t)\rangle, \tag{28}$$

TABLE 1

Damping estimation results for the procedure based on the wavelet transform cross-sections

Example	Frequency (Hz)	Theoretical damping ratio (ζ_t)	Noise level *SNR* (dB)	Estimated damping ratio (ζ_e)	Error (%)
1	20	0·03	∞	0·03001	+0·01
			20	0·02853	−4·90
			10	0·02864	−4·53
	78	0·045	∞	0·04499	−0·01
			20	0·04441	−1·31
			10	0·04441	−1·31
2	25	0·055	∞	0·05477	−0·42
			20	0·05065	−7·91
			10	0·04914	+10·65
	30	0·02	∞	0·02010	+0·50
			20	0·02149	+7·45
			10	0·02359	+17·95

where $\langle x, g \rangle$ is the orthogonal projection of functions $x(t)$ and $g(t)$, $x_a(t)$ is the analytic signal of $x(t)$ is defined as

$$x_a(t) = x(t) + \mathrm{j}\hat{x}(t), \tag{29}$$

and $\hat{x}(t)$ is the Hilbert transform of $x(t)$ given by

$$\hat{x}(t) = \frac{1}{\pi} \int_{-\infty}^{+\infty} x(\tau) \frac{1}{t - \tau} \, \mathrm{d}\tau. \tag{30}$$

The result given by equation (26) was obtained also on the assumption that the analyzing wavelet function has good localization properties in the frequency domain. In practice, when the cross-section of the wavelet transform is used for the particular value of dilation a_a, the Fourier transform of the Morlet wavelet function is peaked at the value of frequency f_0; both values are related by equation (11).

To summarize, the damping estimation procedure can be established as follows: first the cross-section of the wavelet transform of the signal response is obtained, then the result is plotted on an amplitude-time semi-logarithmic scale, and, as a result the damping ratio ζ is obtained. It has to be mentioned that the cross-section of the wavelet transform in the scale domain can be obtained directly from equation (9) without any calculation of the whole time-scale plane. One can see that the procedure based on the wavelet transform is very similar to the procedure based on the classical complex envelope function. The advantage over the classical procedure can be seen when the multi-degree-of-freedom (MDOF) system is analyzed.

The damping estimation procedure based on the wavelet transform, presented above can be extended now to MDOF systems on the assumption that the MDOF systems governed by equation (13), can be uncoupled.

From equations (8) and (25) the response of the MDOF system can be obtained as

$$\left| \left(W_g \sum_{i=1}^{N} x_i \right)(a, b) \right| \approx \sum_{i=1}^{N} A_i \, \mathrm{e}^{-\zeta_i \omega_{n_i} b} \left| G^*(\pm \mathrm{j} a_i \omega_{n_i} \sqrt{1 - \zeta_i^2}) \right|. \tag{31}$$

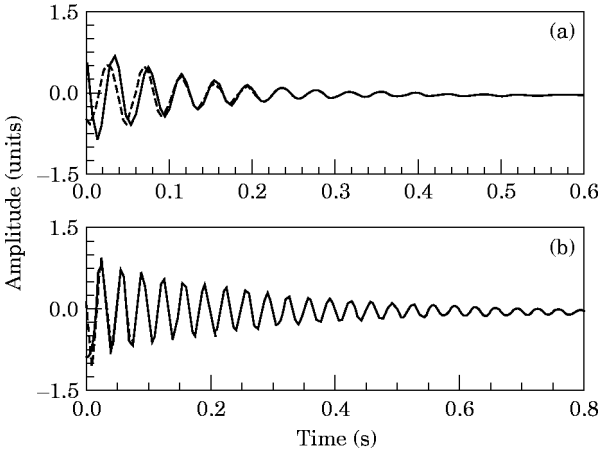

Figure 8. Comparison between theoretical impulse response function (——) and recovered from the wavelet transform impulse response function (– – –). The analysis was performed for the signal from Example 1 representing well separated modes: (a) First mode (20 Hz); (b) second mode (78 Hz).

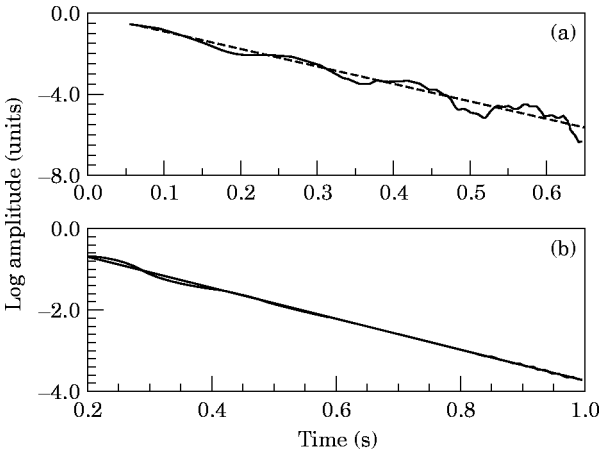

Figure 9. Semi-logarithmic plots (——) of the decaying envelopes of the recovered impulse response functions represented in Figure 8. Linear regression (– – –) was used to obtain the damping ratio. (a) First mode (20 Hz); (b) second mode (78 Hz).

Since the analyzing wavelet function has compact support in the time and frequency domains, for each component x_i,

$$|G^*(\pm \mathrm{j}a_i\omega_{n_i}\sqrt{1-\zeta_i^2})| = 0 \tag{32}$$

for $i = 1, 2, \ldots, i-1, i+1, \ldots, N$. Thus the wavelet transform of each separated mode $i = 1, 2, \ldots, N$ becomes

$$|(W_g x_i)(a, b)| \approx A_i \, \mathrm{e}^{-\zeta_i\omega_{n_i}b}|G^*(\pm \mathrm{j}a_i\omega_{n_i}\sqrt{1-\zeta_i^2})|. \tag{33}$$

Clearly, the wavelet transform offers a decoupling of MDOF systems into single modes. The assumption of vanishing $|G^*(\cdot)|$ in equation (32) depends on the wavelet transform parameters. The wavelet analyzing function for each ith mode is peaked at modal frequency f_i. For the Morlet wavelet function the relationship between frequency and dilation, and the frequency bandwidth of the filter is given by equations (11) and (12), respectively.

TABLE 2

Damping estimation results from Examples 1 *and* 2 *for the impulse response recovery procedure based on the wavelet transform*

Example	Frequency (Hz)	Theoretical damping ratio (ζ_t)	Noise level *SNR* (dB)	Estimated damping ratio (ζ_e)	Error (%)
1	20	0·03	∞	0·03082	+2·73
			20	0·02962	−1·27
			10	0·03102	−3·40
	78	0·045	∞	0·04445	−1·22
			20	0·04450	−1·11
			10	0·04439	−1·36
2	25	0·055	∞	0·05345	−2·82
			20	0·05140	−6·55
			10	0·04647	−15·51
	30	0·02	∞	0·02020	+1·00
			20	0·02065	+3·25
			10	0·02253	+12·65

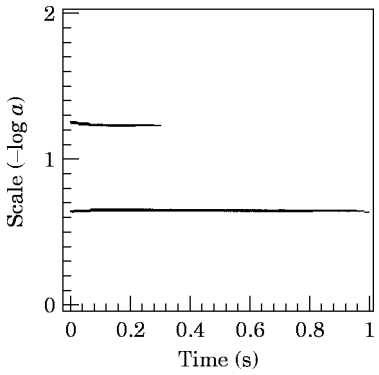

Figure 10. Ridges of the wavelet transform given in Figure 4 representing Example 1.

Following equation (26), the damping ratios ζ_i can now be estimated from equation (33) as the slope of the straight line of the wavelet modulus cross-section $|(W_g x_i)(a_i, b)|$, for the given value of dilation a_i related to the natural frequency f_{n_i} of the system, plotted in a semi-logarithmic scale:

$$\ln |(W_g x_i)(a_i, b)| \approx -\zeta_i \omega_{n_i} b + \ln (A_i |G^*(\pm \mathrm{j} a_i \omega_{n_i} \sqrt{1 - \zeta_i^2})|). \tag{34}$$

It can be seen from equations (26) and (34) that the slopes of the wavelet cross-sections do not depend on the analyzing wavelet function. Obviously in the case of the MDOF systems, in order to decouple the system, the proper choice of the wavelet transform parameters is required to receive a sufficiently compact support in the time and frequency domains.

The advantage of the method over the complex envelope is now clear. The wavelet transform works as a microscope whose optics are given by the wavelet function $g_{a,b}(t)$; magnification by dilation a and position by translation b. This allows decoupling of the MDOF system into single modal components. The contour plots of the wavelet transform give information about time and frequency contents of the signal. The cross-sections of

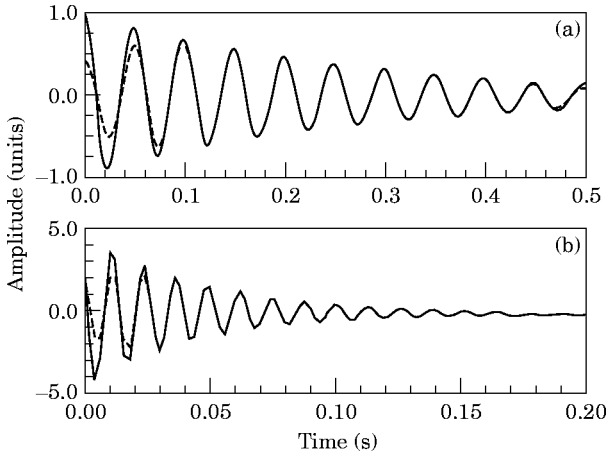

Figure 11. Comparison between real parts of the wavelet transform skeletons (– – –) obtained from the ridges given in Figure 10 and theoretical impulse response function (——) representing well separated modes from Example 1. (a) First mode (20 Hz); (b) second mode (78 Hz).

the wavelet transform offer the possibility of damping identification. The mathematical basis of the method will be illustrated in section 7 by using computer simulations.

5. IMPULSE RESPONSE RECOVERY USING WAVELET RECONSTRUCTION FORMULA

The system can be represented by using the input/output relation

$$\mathbf{Y} = [\mathbf{H}]\mathbf{X}, \tag{35}$$

where $\mathbf{X}$, $\mathbf{Y}$ are the input and output vectors, respectively and $[\mathbf{H}]$ is the impulse response matrix. Existing impulse response extraction procedures involve time or frequency domain calculations. The first approach can apply the observer gain matrix [32] or Kalman filtering [32]. The later approach employs the FFT procedure. More recently an orthogonal wavelet based approach has been proposed [27]. In what follows, an impulse response extraction procedure based on the continuous wavelet transform is used to estimate damping of the system.

The reconstruction formula given by equation (4) can be simplified to obtain a form suitable for numerical calculations [33]:

$$x(t) = \frac{1}{C_g} \int_0^{+\infty} (W_g x)(a, b) \frac{\mathrm{d}a}{a}. \tag{36}$$

This represents a signal as a sum over possible frequencies. The reconstruction formula given by equation (36) together with equation (10) can be used to recover the impulse response function as

$$x(t) = \frac{1}{C_g} \sum_{i=1}^{N} \int_{t - a\Delta t_g}^{t + a\Delta t_g} (W_g x_i)(a, b) \frac{\mathrm{d}a}{a}. \tag{37}$$

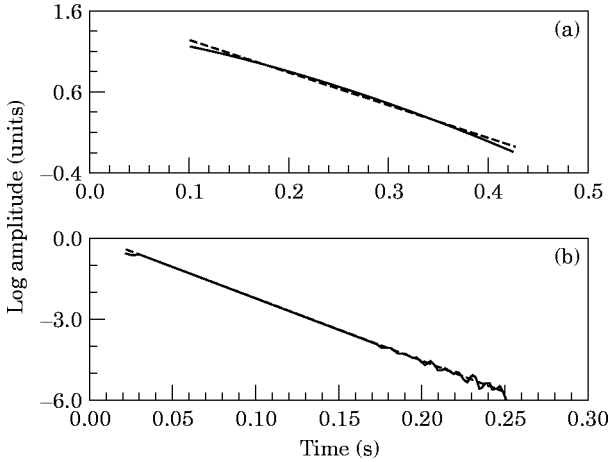

Figure 12. Semi-logarithmic plots (——)of the decaying envelopes of the skeleton real parts given in Figure 11. Linear regression (– – –) was used to obtain the damping ratio. (a) First mode (20 Hz); (b) second mode (78 Hz).

TABLE 3

Damping estimation results from Examples 1 *and* 2 *for the procedure based on the ridges and skeletons of the wavelet transform*

Example	Frequency (Hz)	Theoretical damping ratio (ζ_t)	Noise level *SNR* (dB)	Estimated damping ratio (ζ_e)	Error (%)
1	20	0·03	∞	0·03019	+0·63
			20	0·02884	−3·87
			10	0·02876	−4·13
	78	0·045	∞	0·04447	−1·18
			20	0·04410	−2·00
			10	0·04690	−4·22
2	25	0·055	∞	0·05365	−2·45
			20	0·05263	−4·31
			10	0·05230	−4·91
	30	0·02	∞	0·02005	+0·03
			20	0·02050	+2·50
			10	0·02070	+3·50

This can be simplified for a single mode i as

$$x(t) = \frac{1}{C_{g_i}} \int_{t - a\Delta t_g}^{t + a\Delta t_g} (W_g x_i)(a, b) \frac{\mathrm{d}a}{a}, \tag{38}$$

where

$$C_{g_i} = \int_{f_i - \Delta f_g/a}^{f_i + \Delta f_g/a} \frac{|G(f)|^2}{|f|} \mathrm{d}f. \tag{39}$$

The time-scale decomposition preserves the temporal nature of the vibration data during the filtration operation due to the character of the wavelet transform and signal reconstruction formula. The damping estimation procedure is now straightforward. The impulse response function for a single mode can be recovered from the wavelet transform by using equation (38). The damping ratio ζ can be then estimated as a slope of the semi-logarithmic plot of the impulse response function envelope from equation (21).

6. RIDGES AND SKELETONS OF THE WAVELET TRANSFORM

The square of the modulus of the wavelet transform can be interpreted as an energy density distribution over the (a, b) time-scale plane. The energy of a signal is mainly concentrated on the time-scale plane around the so called ridges of the wavelet transform.

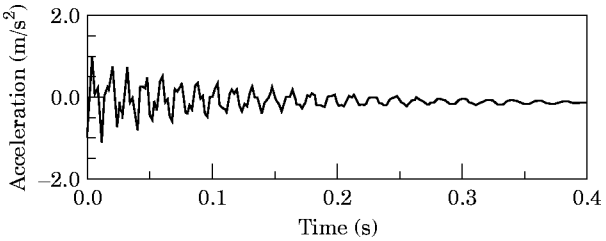

Figure 13. Impulse response functions for the signal exhibiting varying frequency contents and analyzed in Example 3.

The concept of a ridge can be developed from the analytic representation of a signal given by equation (29), which can be rewritten as

$$a(t) = x(t) + \mathrm{j}\hat{x}(t) = A(t)\,\mathrm{e}^{\mathrm{j}\phi(t)}, \tag{40}$$

where $\hat{x}(t)$ is the Hilbert transform of the signal $x(t)$ and $A(t)$, $\phi(t)$ are the envelope and the instantaneous phase of the signal, respectively. Suppose that the signal and the wavelet are asymptotic, which means they have slowly varying amplitudes compared with phase variations. Let t_s also denote some stationary points of [33]

$$\overline{\phi}_{a,b}(t) = \phi_x(t) - \phi_g(t-b)/a. \tag{41}$$

Here ϕ_x and ϕ_g denote instantaneous phases of the signal and the wavelet. Mathematically the ridge of the function is the curve $a = r(b)$, which consists of points (a, b), satisfying the condition $t_s(a, b) = b$ [33]. This means in practice that the wavelet transform gives the contributions of such stationary points to the scalar product between the signal and the wavelet in equation (2). The important property of the ridge is that it is directly related to the instantaneous frequency of the signal. This relationship, which follows from the ridge definition is given by [33]

$$r(b) = \dot{\phi}_g(0)/\dot{\phi}_x(b). \tag{42}$$

The values of the wavelet transform restricted to its ridge are called the skeleton of the wavelet transform. It can be shown that the skeleton of the wavelet transform can be expressed as [33]

$$(W_g x)(r(b), t) = C(t)a(t), \tag{43}$$

where $C(t)$ is the correction function completely determined by the wavelet and the ridge. This means in practice that the signal and its Hilbert transform are given approximately by the real and imaginary parts of the skeleton of the wavelet transform, respectively.

There exist different algorithms for ridge extraction. The most usual uses the local maxima of the amplitude of the transform. This algorithm gives exact values only for linear ridges. A better way of extraction can be obtained from the phase function; this algorithm was proposed by Tchamitchian and Torresani [33]. The algorithm uses the following properties of the ridge [33],

$$\partial\Omega(a, b)/\partial a = 0, \text{ and } [\mathrm{d}\Omega(a, b)/\mathrm{d}b]_{t_s(a,b)=b_0} = \dot{\phi}_g(0)/a \tag{44}$$

on the ridge and on the intersection with the ridge, respectively. Here $\Omega(a, b)$ is the phase of the wavelet transform. For more detailed analysis related to ridges and skeletons of the wavelet transform the reader is referred to reference [33].

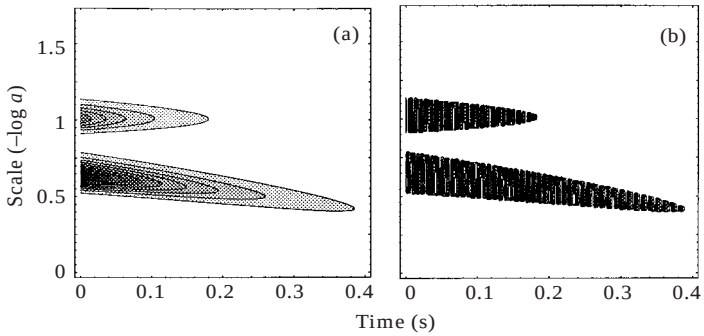

Figure 14. Wavelet transform for the signal from Example 3 given in Figure 13. (a) Amplitude; (b) phase.

The ridge and skeleton of the wavelet transform can be detected separately for each mode. Thus the skeleton of the wavelet transform gives the impulse response function and its Hilbert transform. This can be used to obtain the envelope function of the impulse response for each single mode and, following equation (21), to estimate the damping of the system.

7. EXAMPLES OF DAMPING IDENTIFICATION

7.1. SIMULATED RESULTS

In order to show the usefulness of the damping estimation procedures, simulations were performed. The algorithms based on the wavelet transform were coded in C and implemented on a SUN workstation. The wavelet transform was calculated in the frequency domain as a bank of filters based on the Morlet analysing wavelet. The details of this implementation can be found in reference [34].

For simplicity the impulse response of the two-degree-of-freedom (2-DOF) system was simulated. However, it is assumed that the procedures can be used for general MDOF systems. The simulated data was corrupted by zero mean Gaussian noise. The signal-to-noise ratio (SNR), in terms of *rms* values, was equal to 20 dB and 10 dB. The results are presented below.

Example 1. The first example analyzed involved a 2-DOF system with well separated modes. The IRF consisted of two exponentially decaying sine waves with frequencies equal to 20 Hz and 78 Hz. The damping ratios were equal to 0·03 and 0·045 respectively.

Example 2. A 2-DOF system with close modes was analyzed as the second example. The IRF included two exponentially decaying sine waves with frequencies equal to 25 Hz and 30 Hz. The relative frequency difference between modes compared with the sampling frequency used, represents a typical mode interaction in an aircraft structure data [26].

The IRFs and FRFs of the simulated signals are given in Figures 2 and 3 respectively. Figure 4 shows the wavelet transform for Example 1. The wavelet transform is given in the form of the contour plots of its amplitude and phase. Two modes are represented by two horizontal dark bands in the modulus and two horizontal bands with parallel vertical stripes in the phase. Each pattern is produced by a sine wave. The decaying nature due

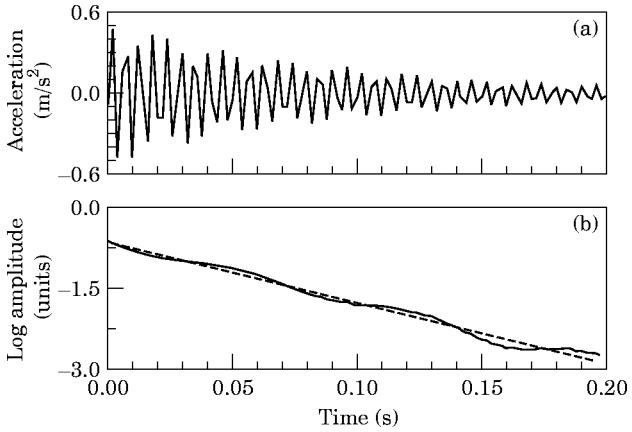

Figure 15. Impulse response function recovery procedure based on the wavelet transform and performed for the impulse response function from Example 3: (a) High frequency mode; (b) semi-logarithmic plot (——) of the recovered impulse response function decaying envelope. Linear regression (– – –) was used to obtain the damping ratio.

to the exponential decay of the sine wave can also be observed. The values of the phase change from 0 to 2π. When the phase reaches 2π, it is wrapped around to the value 0. The vertical stripes represent lines of constant phase. The wavelet transform for Example 2 is given in Figure 5. Here, two close modes which are difficult to observe in Figure 5(a,b) can be clearly separated using a shifted ($f_h = 15$ Hz) Morlet wavelet function in Figure 5(c,d).

The procedure involving the wavelet transform cross-section was used to identify the damping ratios. The cross-sections of the wavelet transform were obtained for the values of dilation related to the analyzed modal frequencies. The semi-logarithmic plots of these cross-sections were used to estimate damping ratios. Figure 6 shows an example of the wavelet transform amplitude cross-sections representing the IRF with two close modes from Example 2. Here, the wavelet transform from Figure 5(c,d) was used to obtain the cross-sections representing close modes. The semi-logarithmic plots of these cross-sections are given in Figure 7. Linear regression was used to obtain the damping ratio from the semi-logarithmic plots. Estimated values of damping are given in Table 1 for different frequency modes and levels of Gaussian white noise added to the data.

The wavelet reconstruction formula was used to recover the IRFs. The values of damping were estimated from the IRFs by using decaying envelopes. Figure 8 shows a comparison between theoretical (solid line) and recovered from the wavelet transform (dashed line) IRFs representing well separated modes from Example 1. These two curves show good agreement apart from the beginning of the data. The accuracy of the recovery procedure can be evaluated by using the normalised Mean Square Error (MSE) defined as [35]

$$MSE(x) = \frac{100}{N\sigma_x^2} \sum_{i=1}^{N} (x_i - \hat{x}_i)^2, \tag{45}$$

where x_i is the theoretical impulse response function, $\hat{x}_i$ is the recovered impulse response function, σ_x is the standard deviation of the theoretical impulse response function and N is the number of sample points in the analyzed data. The MSE for the example presented is equal to 23·5%. However, when the 15% of the signal beginning is not taken into account, the MSE reaches 0·41%. Figure 9 shows the semi-logarithmic plots of the decaying envelopes of the recovered IRFs. Linear regression was used to obtain damping ratios from the semi-logarithmic plots. Table 2 gives estimated values of damping for different frequency modes and levels of Gaussian white noise used to corrupt the original data.

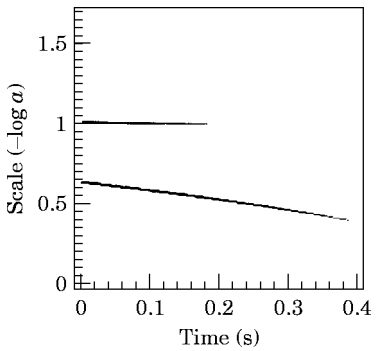

Figure 16. Ridges of the wavelet transform given in Figure 14 representing Example 3.

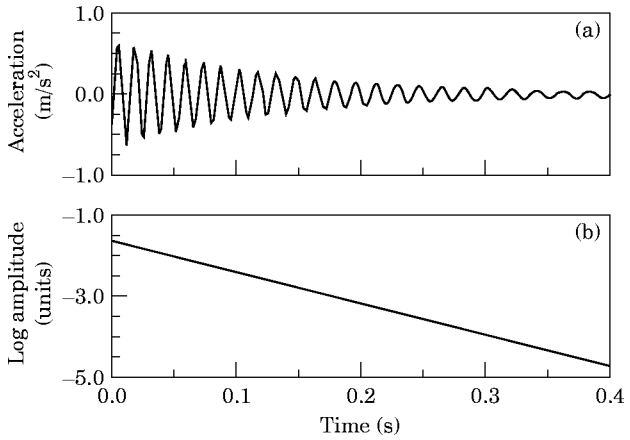

Figure 17. Damping estimation procedure based on the ridges and skeletons of the wavelet transform and performed for the impulse response function from Example 3: (a) Real part of the wavelet transform skeleton obtained from the ridge representing the low frequency mode; (b) semi-logarithmic plot of the real part of the wavelet transform skeleton obtained from the ridge representing the low frequency mode.

Finally, the ridges and skeletons of the wavelet transform were used to estimate damping of the system. Figure 10 shows the ridge of the wavelet transform for Example 1. The ridge consists of two parts representing two frequency modes. The wavelet transform skeletons were obtained from this ridge separately for each mode. Figure 11 gives a comparison between real parts of the wavelet transform skeletons (dashed lines) obtained from the ridges given in Figure 11, and the theoretical IRFs (solid line) representing well separated modes from Example 1. This, apart from the ends, shows perfect match of both signals. The MSE for this example is equal to 35·7%; however, when the 15% of the signals at both ends are rejected, the MSE reaches 0·74%. The damping ratios were estimated by using the skeleton of the wavelet transform. Figure 12 shows the semi-logarithmic plots of the decaying envelopes of the skeleton real parts presented in Figure 11. Linear regression was used to obtain damping ratio from these plots. The estimated values of damping for different frequency modes and levels of noise are given in Table 3.

Example 3. The third example analyzed involved a 2-DOF system with varying frequency content. The simulated signal consists of two frequency modes: high frequency sine wave (180 Hz) with exponential decay, low frequency sine wave (4 Hz) with exponential decay and linearly varying frequency (4–8 Hz). The damping ratios of these two modes were equal to 0·3 and 0·01 respectively.

TABLE 4

Damping estimation results from Example 3 *for the impulse response recovery procedure based on the wavelet transform*

Example	Frequency (Hz)	Theoretical damping ratio (ζ_t)	Noise level *SNR* (dB)	Estimated damping ratio (ζ_e)	Error (%)
3	varying	0·03	∞	0·02995	−0·17
			20	0·03054	+1·80
			10	0·03543	+18·30
	180	0·01	∞	0·01026	+2·60
			20	0·00955	−4·51
			10	0·00946	−5·39

TABLE 5

Damping estimation results from Example 3 for the procedure based on the ridges and skeletons of the wavelet transform

Example	Frequency (Hz)	Theoretical damping ratio (ζ_t)	Noise level *SNR* (dB)	Estimated damping ratio (ζ_e)	Error (%)
3	varying	0·03	∞	0·03012	+0·40
			20	0·03063	+2·10
			10	0·03151	+5·03
	180	0·01	∞	0·00992	−0·81
			20	0·00973	−2·71
			10	0·00967	−3·30

Figure 13 shows the simulated IRFs from Example 3. The wavelet transform of the signal is presented in Figure 14. The amplitude and phase of the wavelet transform exhibits similar behaviour to that observed in Figures 4 and 5. The varying frequency contents of the low frequency mode can be seen additionally.

The IRF recovery procedure and ridges of the wavelet transform were used to estimate the damping ratios. Figure 15(a) shows an example of the recovered IRF for the high frequency component. The semi-logarithmic plot of the decaying envelope of this IRF can be seen in Figure 15(b). The ridge of the wavelet transform is given in Figure 16. Figure 17(a) gives the real part of the skeleton of the wavelet transform representing low frequency mode. The semi-logarithmic plot of the decaying envelope of the wavelet transform skeleton is presented in Figure 17(b). Table 4 gives the values of the damping ratios for different modes and levels of noise. Here the impulse response function recovery procedure was used to estimate damping. Similar results using ridges and skeletons of the wavelet transform are shown in Table 5.

7.2. DISCUSSION AND FINAL REMARKS

Three different techniques based on the wavelet transform were used to estimate damping of 2-DOF systems. The cross-section procedure is easy to use. It does not require any calculations in the whole time-scale wavelet transform domain. However the limitations come from the fact that it can be used only for linear systems with constant frequency. It can be seen in Table 1 that the accuracy of damping estimation is very good for systems with well separated modes. The error remains less than 5% even for the data corrupted by the noise. In the presence of close modes, the noise effects the results significantly.

The impulse response function can be recovered by using the wavelet transform. The procedure involves the process of filtering in the time-scale domain. The results presented in Figure 8 show that the impulse response can be recovered with good accuracy apart from the beginning of the signal. The disturbances at the beginning of the signal result from the process of filtering and are similar to the well known Gibbs phenomenon. Damping of the system can be estimated from the recovered impulse response function. Estimated damping values presented in Tables 2 and 4 show that the impulse recovery method is as effective as the cross-section procedure in the case of the well separated modes and performs better in the case of the close mode systems. The method offers additionally the possibility of damping estimation for systems with varying frequency contents. It failed only in the case of noisy data ($SNR = 10$ dB).

The impulse response function can also be recovered by using the ridge and skeleton of the wavelet transform. The procedure is based on the phase of the wavelet transform. The recovery results presented in Figure 11 are in good agreement with the theoretical impulse response functions, apart from the ends of the signal. The disturbances are due to the ridge detection procedure which is based on the phase of the wavelet transform. The lines of constant phase are curved in such a way that their maxima lay at their intersections with the ridge. Thus the ridge detection procedure requires a stationary phase approximation, which fails at the end of the signal. However, the damping estimation results presented in Tables 3 and 5 show very good accuracy. The error is less or equal than 5% even in the case of noisy data and two close modes or varying frequency contents. There is still a margin for further improvement when the amplitude of the wavelet transform is used to detect the ridge [31].

It has to be mentioned that standard methods of damping estimation based on the complex envelope and Hilbert transform can offer similar results especially in the case of the cross-section procedure. However the main interest of the wavelet transform-based analysis is in the context of filtering, which in the case of classical methods is performed in the time or frequency domain, and in the case of the wavelet transform analysis is realized in the combined time-scale domain. This allows one to use the method for a combination of asymptotic signals which in practice represent non-linear and time-variant behaviour of the system.

8. CONCLUSIONS

Three methods of damping identification based on the time-scale decomposition have been presented. The methods use the continuous wavelet transform to unfold the multicomponent structure of the MDOF system impulse response. The wavelet transform has been used to decouple the system into single harmonic modes. The mathematical framework of the decoupling procedure has been provided. It has been shown that the methods are independent of the choice of the analyzing wavelet function. The three damping estimation procedures which have been presented are: the wavelet transform cross-section procedure, the impulse response recovery procedure based on wavelet domain filtering and the ridge detection procedure. The procedures have been applied to simulated 2-DOF systems giving satisfactory results of damping estimation. Out of the three procedures the wavelet ridge detection technique gives the best accuracy especially in the case of noisy data.

More work involving simulated and experimental results is required to fully establish the methods. Further work is directed to modal parameter identification in linear and non-linear systems.

ACKNOWLEDGMENT

The author is very grateful to Dr. Keith Worden from Sheffield University for his valuable comments and discussions.

REFERENCES

1. B. J. Lazan 1968 *Damping of Materials and Members in Structural Mechanics*. Oxford: Pergamon Press.
2. D. J. Ewins 1984 *Modal Testing*: *Theory and Practice*. Letchworth, Herts., England: Research Studies Press Ltd.

3. W. T. Thomson 1993 *Theory of Vibration with Applications*. London: Chapman and Hall (fourth edition).
4. D. I. G. Jones 1987 in *Shock & Vibration Handbook* (editor C. M. Harris); New York: McGraw-Hill. Application of damping treatments (third edition).
5. L. E. Goodman 1987. In Harris C. M. editor, *Shock & Vibration Handbook*. New York: McGraw-Hill. Material damping and slip damping (third edition).
6. J. Van Tomme 1988 In 13*th International Seminar on Modal Analysis*, *Katholieke Universiteit Leuven*, *Belgium*, 19–23 September. Evaluation of damping measurements in materials and structures.
7. J. E. Cooper 1995 *AGARD*, *SMP Meeting*, *Rotterdam*, *May*. Parameter estimation methods for flutter testing.
8. A. Tondl 1975 *Shock and Vibration Digest*, **7**, 3–17. The application of skeleton curves and limit envelopes to analysis of nonlinear vibration.
9. J. K. Lee and Y. S. Park 1992 *Proceedings of the* 10*th IMAC*, *San Diego*, *California*, 167–172. Modal parameter estimation in structural system using complex envelope signal.
10. D. Spina, F. Brancaleoni and C. Valente 1992 *International Workshop on Safety Evaluation of Time-Variant and Nonlinear Structures Using Identification Approaches*., *Lambrecht*, *Germany*, 6–9 *September*. Damage assessment from the dynamic response of deteriorating structures.
11. M. Feldman 1994 *Mechanical Systems and Signal Processing* **8**, 119–127. Nonlinear system vibration analysis using the Hilbert transform—i. free vibration analysis method freevib.
12. M. Feldman 1994 *Mechanical Systems and Signal Processing*, **8**, 309–318. Nonlinear system vibration analysis using Hilbert transform—ii. forced vibration analysis method forcevib.
13. M. Feldman and S. Braun 1995 In *Proceedings of* 13*th IMAC*, *Nashville*, *Tennessee*. pp. 637–642. Identification of nonlinear system parameters via the instantaneous frequency: application of the Hilbert transform and Wigner–Ville techniques.
14. D. Gabor 1946 *Journal of the Institution of Electrical Engineers* **93**, 429–457. Theory of communication.
15. C. W. Helström 1966 *IEEE Transactions on Information Theory*. IT-12: 81–82. An expansion of a signal in gaussian elementary signals.
16. J. Morlet 1980 In *Proceedings of the* 51*st Annual Meeting Soc*. *Explor*. *Geophys*. *Los Angeles*. Sampling theory and wave propagation.
17. A. Grossman and J. Morlet 1985 In *Mathematics and Physics*, *Lecture on Recent Results* (Editor L. Streit). Singapore: World Scientific.
18. A. P. Calderon 1964 *Stud*. *Math* **24**, 113–190. Intermediate spaces and interpolation, the complex method.
19. D. Esteban and C. Galand 1977 Application of the quadrature mirror filters to split band voice coding schemes. In *Proceedings of IEEE ICASSP* 77 191–195.
20. Y. Meyer 1993 *Wavelets*. *Algorithms & Applications*. Philadelphia: SIAM.
21. Ch. K. Chui 1992 *An Introduction to Wavelets*. Wavelet Analysis and its Applications volume 1. Boston: Academic Press.
22. A. K. Louis In *Proceedings of the International Workshop on Inverse Problems*, *Hannover University*, *Germany*, 67–75. A wavelet approach to identification problems.
23. D. E. Newland 1993 *Random Vibration*, *Spectral and Wavelet Analysis*. New York: Longman, Harlow and John Wiley, third edition.
24. S. Y. Huang, G. Z. Qi and J. C. S. Yang 1994 In *Proceedings of* 12*th IMAC*, *Honolulu*, *Hawaii*, 1162–1166. Wavelets for system identification.
25. R. D. Priebe and G. R. Wilson 1994 In *Proceedings of the IEEE International Conference on Acoustics*, *Speech and Signal Processing*, *Adelaide*, *Australia*, **III**, 205–208. Wavelet applications to structural analysis.
26. W. J. Staszewski and J. E. Cooper 1995 In *Proceedings of the International Congress MV*2: *New Advances in Modal Synthesis of Large Structures*, *Nonlinear*, *Damped and Non-deterministic Cases*, *Lyon*, *France*, 5–6 *October*, 549–561. Flutter data analysis using the wavelet transformation.
27. K. C. Park, A. N. Robertson and K. F. Alvin 1995 In *Proceedings of the Design Engineering Technical Conference*, *DE*-84.1 *ASME*-95, 1323–1334. Extraction of impulse response data via wavelet transform for structural system identification.
28. R. Kronland-Martinet and J. Morlet 1987 *International Journal of Pattern Recognition and Artificial Intelligence* **1**, 273–302. Analysis of sound through wavelet transforms.
29. W. J. Staszewski and G. R. Tomlinson 1994 *Mechanical Systems and Signal Processing* **8**, 289–307. Application of the wavelet transform to fault detection in a spur gear.

30. R. N. BRACEWELL 1978 *The Fourier Transform and its Application*. New York: McGraw-Hill (second edition).
31. W. L. HWANG, R. A. CARMONA and B. TORRESANI 1995 Characterization of signals by the ridges of their wavelet transforms. *Preprint* 1994.
32. J. N. JUANG 1994 *Applied System Identification*. Englewood Cliffs, NJ: Prentice-Hall.
33. Ph. TCHAMITCHIAN and B. TORRESANI 1992 *In Wavelets and their Applications*, editor, M B Ruskai. Boston: Jones and Bartlett. Ridge and skeleton extraction from the wavelet transform.
34. W. J. STASZEWSKI 1994 *PhD Thesis*, *University of Manchester*. The application of time-variant analysis to gearbox fault detection.
35. K. WORDEN 1990 *Mechanical Systems and Signal Processing* **4**, 295–319. Data processing and experiment design for the restoring force surface method, part 1: integration and differentiation of measured time data.